Understanding the origin of disorder in kesterite-type chalcogenides A2ZnBQ4 (A = Cu, Ag; B = Sn, Ge; Q = S, Se): the influence of inter-layer interactions

Article

Accepted Version

PCCP
Physical Chemistry Chemical Physics

Accepted Manuscript

This article can be cited before page numbers have been issued, to do this please use: P. Mangelis, A. Aziz, I. da Silva, R. Grau-Crespo, P. Vaqueiro and A. V. Powell, *Phys. Chem. Chem. Phys.*, 2019, DOI: 10.1039/C9CP03630J.

ROYAL SOCIETY OF CHEMISTRY

rsc.li/pccp

View Article Online
DOI: 10.1039/C9CP03630J

Understanding the Origin of Disorder in Kesterite-type Chalcogenides A_2ZnBQ_4 (A = Cu, Ag; B = Sn, Ge; Q = S, Se): the Influence of Inter-layer Interactions

Panagiotis Mangelis,[a] Alex Aziz,[a] Ivan da Silva,[b] Ricardo Grau-Crespo,[a] Paz Vaqueiro[a] and Anthony V. Powell*[a]

[a] *Department of Chemistry, University of Reading, Whiteknights, Reading RG6 6AD, England, United Kingdom*

[b] *STFC, Rutherford Appleton Laboratory, ISIS Facility, Didcot OX11 0QX, United Kingdom*

View Article Online
DOI: 10.1039/C9CP03630J

Abstract

Semiconducting quaternary chalcogenides with A_2ZnBQ_4 stoichiometry, where A and B are monovalent and tetravalent metal ions and Q is a chalcogen (e.g. Cu_2ZnSnS_4 or CZTS) have recently attracted research attention as potential solar-cell absorbers made from abundant and non-toxic elements. Unfortunately, they exhibit relatively poor sunlight conversion efficiencies, which has been linked to site disorder within the tetrahedral cation sub-lattice. In order to gain a better understanding of the factors controlling cation disorder in these chalcogenides, we have used powder neutron diffraction, coupled with Density Functional Theory (DFT) simulations, to investigate the detailed structure of A_2ZnBQ_4 phases, with A = Cu, Ag; B = Sn, Ge; and Q = S, Se. Both DFT calculations and powder neutron diffraction data demonstrate that the kesterite structure (space group: $\overline{I4}$) is adopted in preference to the higher energy stannite structure (space group: $I\overline{4}2m$). The contrast between the constituent cations afforded by neutron diffraction reveals that copper and zinc cations are only partially ordered in the kesterites Cu_2ZnBQ_4 (B = Sn, Ge), whereas the silver-containing phases are fully ordered. The degree of cation order in the copper-containing phases shows a greater sensitivity to the identity of the *B-c*ation than to the chalcogenide anion. DFT indicates that cation-ordering minimises inter-planar $Zn^{2+}\cdots Zn^{2+}$ electrostatic interactions, while there is an additional intra-planar energy contribution associated with size mismatch. The complete Ag/Zn order in Ag_2ZnBQ_4 (B = Sn. Ge) phases can thus be related to the anisotropic expansion of the unit cell on replacing Cu with Ag.

View Article Online
DOI: 10.1039/C9CP03630J

Introduction

There is a high level of interest in quaternary chalcogenides of general formula A_2BCQ_4 (where *A*, *B* and *C* are elements from groups 11, 14 and 12 respectively and *Q* = S, Se) in relation to sustainable energy technologies.[1] For example, thin-film solar cells constructed from Cu_2ZnSnQ_4 exhibit remarkable efficiencies of around 12.6%.[2] Although this is somewhat reduced from that of $CuInGaSe_2$ (CIGS) based devices, the Earth abundance of the constituent elements, obviates the need for the comparatively rare and expensive elements, indium and gallium. The quaternary chalcogenides also show promise as intermediate temperature thermoelectrics,[3,4] owing to their characteristically low thermal conductivities However, they exhibit low electrical conductivities and hole doping, through chemical substitution, is required to increase the charge-carrier concentration and tune the TE properties.[4,5,6] For example, copper-substituted $Cu_2ZnSnSe_4$ reaches ZT ≈ 0.9 at 860 K[7] This may be the result of enhanced phonon scattering, arising from the variation in metal-chalcogen distance of tetrahedrally-coordinated cations. In addition, Ru-loaded A_2ZnBS_4 (*A* = Cu, Ag; *B* = Sn, Ge) is an effective photocatalyst for water splitting under visible light.[8]

Similar to the chalcopyrite structure of CIGS, A_2BCQ_4 quaternary phases crystallise in an ordered superstructure of zinc blende, with the majority of reports describing the room-temperature structure as being either of the stannite ($I\bar{4}2m$) or kesterite ($I\bar{4}$) type. The two structures (Figure 1) differ in the ordering of cations over the available tetrahedral sites: the principal difference being the presence of *A* cations within every cation plane (2*a* and 2*c* sites) in the unit cell of the kesterite structure but only in planes located at *z* = 0.25 and 0.75 (4*d* sites) in the stannite structure.

The lower efficiency of $Cu_2ZnSnS(Se)_4$ photovoltaic devices compared to their CIGS counterparts is associated with a low open-circuit voltage, V_{oc}.[9] The origin of this

View Article Online
DOI: 10.1039/C9CP03630J

limitation on performance remains poorly understood. It has been proposed that both band tailing due to electrostatic potential fluctuations[10] and spatial fluctuations in band-gap due to cation disorder may play a role,[11] although it has also been suggested that the latter has negligible impact on V_{oc}.[12] Detailed structural characterization is therefore of fundamental importance in understanding the underlying factors limiting the efficiency of quaternary chalcogenide photovoltaics and hence realising the efficiency gains required to create cost-effective high-efficiency devices.

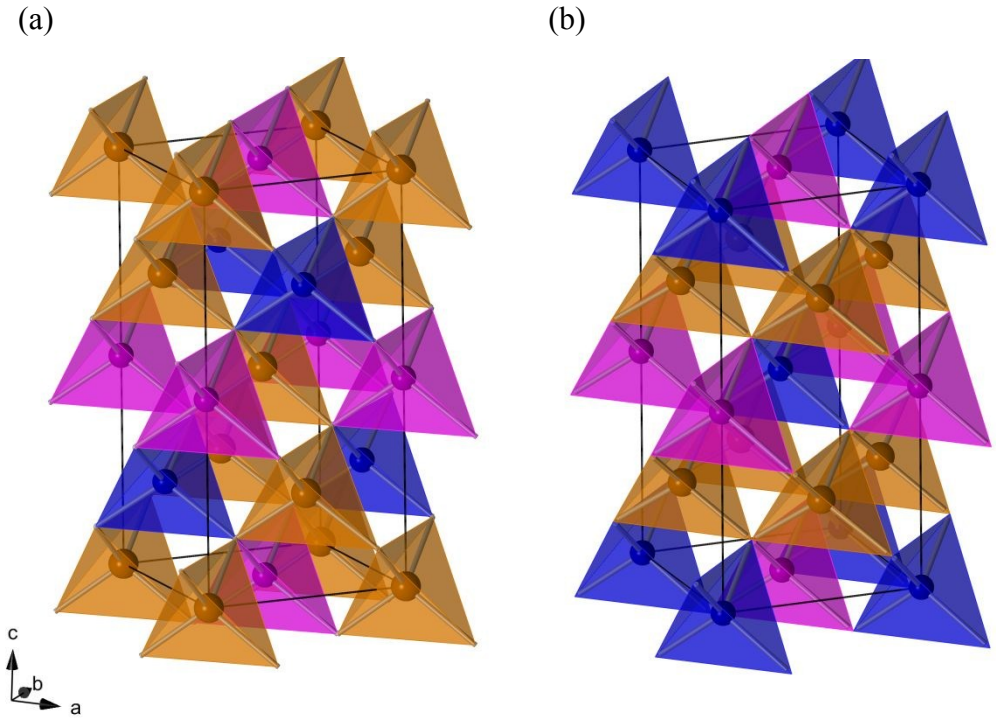

Figure 1 Polyhedral representation of (a) the kesterite structure and (b) the stannite structure of general formula A_2BCQ_4. *A*-, *B*- and *C*- centered tetrahedra are denoted by orange, magenta and blue shading respectively.

Despite several structural investigations on this family of materials, ambiguity remains over detailed structural descriptions. This may be traced to the similarity of the lattice parameters of the two structure types, together with the lack of any discrimination between the $(I\bar{4}2m)$ and $(I\bar{4})$ space groups through systematic absences. Significantly

View Article Online
DOI: 10.1039/C9CP03630J

the constituent cations of many of the phases also have similar X-ray scattering powers, further hampering efforts to establish detailed structures by X-ray methods. Additional confusion arises over the use of the terms stannite and kesterite in the literature. Here, we take stannite to denote an ordered configuration described in the space group $I\bar{4}2m$. Cation disorder can give rise to structures also described in $I\bar{4}2m$, which are neither stannite nor kesterite, while alternative *A*/*B* ordering schemes give to rise to structures described in different space groups.[13]

The majority of investigations have focused on $Cu_2ZnSnS(Se)_4$ phases, owing to their importance to photovoltaic applications. Many of these reports identify stoichiometric $Cu_2ZnSnS(Se)_4$ phases as kesterite-type,[14,15,16,17] while in other reports they are described as stannite.[7,18,19,20] The closely related $Cu_2ZnGeS(Se)_4$ phases have also been reported to crystallize in the stannite structure.[4,21,22] Chen *et al.*[23,24] have shown that the most stable configuration of $Cu_2ZnSnS(Se)_4$ is the ordered kesterite structure but small energy differences could lead to both the stannite and the disordered configurations being present in experimental samples.[11, 12] Whilst materials in the series $Cu_2ZnGeSe_{4-x}S_x$ have been described as crystallizing in the stannite structure, ^{63}Cu nuclear magnetic resonance (NMR)[25] indicates at least two distinct sites for Cu atoms in $Cu_2ZnGeSe_4$ at room temperature, which is inconsistent with the adoption of a structure described in $I\bar{4}2m$. Schorr[26] has shown by powder neutron diffraction that $Cu_2ZnSnS(Se)_4$ phases adopt the kesterite structure; a conclusion supported by Raman scattering.[27] The kesterite structure has been shown to persist into off-stoichiometric materials.[28,29, 30,31] It has been proposed that the V_{oc} limit can be overcome by silver substitution in $Cu_2ZnSnS(Se)_4$,[32] although experimental results so far are contradictory.[1]

Here we adopt a combined experimental-computational approach which exploits the contrast provided by neutrons, together with DFT calculations, to establish the room

View Article Online
DOI: 10.1039/C9CP03630J

temperature structure of A_2ZnBQ_4 (A = Cu, Ag; B = Sn, Ge and Q = S, Se) phases. The results demonstrate that whilst each is best described in the kesterite $(I\bar{4})$ structure, which DFT calculations confirm is energetically favoured over the stannite $(I\bar{4}2m)$ form for all compositions, the detailed structures, in particular the degree of cation order, show a marked compositional dependence that may be traced to the impact of next-nearest neighbour inter-layer interactions.

Methodology

Experimental

With the exception of $Ag_2ZnSnSe_4$ which was prepared by a mechanochemical method, all materials were prepared by high-temperature synthesis from appropriate mixtures of the powdered elements, loaded into evacuated silica ampoules. Full details are provided in the ESI.† For the preparation of $Ag_2ZnSnSe_4$, stoichiometric amounts of powdered elements were sealed, under an argon atmosphere into a 25 mL stainless steel jar together with thirty 6 mm diameter steel balls. The mixture was milled for 4 h at 600 rpm using a Retsch PM100 planetary ball mill and subsequently annealed at 500 °C for 30 min in an evacuated and sealed fused silica tube.

Initial structural characterization was carried out by powder X-ray diffraction using a Bruker D8 Advance diffractometer (Ge-monochromated Cu Kα_1, λ = 1.5406 Å) fitted with a LynxEye linear detector. Room-temperature powder neutron diffraction data[33] were collected at the ISIS facility, Rutherford Appleton Laboratory, using the GEM diffractometer. Samples were contained in vanadium cans. Multibank Rietveld refinements incorporating data from banks at 2θ = 156°, 90°, 63° and 35° were performed using the GSAS software package.[34] In the case of the silver-containing

† Electronic Supplementary Information is available.

View Article Online
DOI: 10.1039/C9CP03630J

materials, powder X-ray diffraction data were included in simultaneous X-ray/neutron refinements in order to improve the contrast between Ag and Zn, owing to their similar neutron scattering lengths (b(Zn) = 5.7, b(Ag) = 5.9 fm). All multibank refinements were carried out using, for the initial structural models, lattice parameters and atomic coordinates determined from powder X-ray diffraction.

Computational

Density functional theory (DFT) calculations were performed using the VASP code,[35, 36,37] employing the screened hybrid Heyd, Scuseria and Ernzerhof (HSE06)[38,39] exchange-correlation functional. This provides an improved description of the electronic structure of transition-metal oxides and sulphides, in comparison with local and semi-local functionals.[40] Structures were relaxed until the forces on the atoms were minimized to less than 0.01 eV/Å. The projector augmented wave (PAW) method[41,42] was used to describe the interaction of valence electrons with the cores, which consist of frozen levels up to 2*p* for S; up to 3*p* for Cu, Zn, Ge and Se; and up to 4p for Ag and Sn. The kinetic energy cut-off for the plane-wave basis set expansion was set at 410 eV (30% above the value required by the PAW potentials, in order to avoid Pulay errors). A 2×2×1 mesh of k-points was used for reciprocal-space sampling in the unit cell and zone-centre only sampling was used for the 2×2×1 supercells. Test calculations doubling the k-point grid density showed that energy differences between configurations were converged to within 2-3 meV per 16-atom cell."

Cu/Zn disorder was modelled using a symmetry adapted ensemble of configurations, as implemented in the SOD (Site Occupancy Disorder) program.[43] In the conventional unit cell, this allowed for five inequivalent configurations for each composition. Further analysis conducted with a 2×2×1 supercell generated 255 possible inequivalent

View Article Online
DOI: 10.1039/C9CP03630J

configurations for each composition. Restricting the possibilities to in-plane disorder reduces the number of calculations to only 108 of the 255 possible configurations.

Results and Discussion

Initial structural characterization by powder X-ray diffraction shows Cu_2ZnGeS_4, $Cu_2ZnGeSe_4$ and Ag_2ZnSnS_4 to be single-phase materials. Trace amounts of SnS and SnSe are evident in Cu_2ZnSnS_4 and $Cu_2ZnSnSe_4$, respectively, while similarly low levels of $SnSe_2$ and ZnSe are detectable in the powder X-ray diffraction pattern of $Ag_2ZnSnSe_4$. Rietveld refinements using the powder X-ray diffraction data were carried out to determine lattice parameters and the basic structural details of the materials. As noted above, the almost identical X-ray scattering powers of Cu^+ and Zn^{2+} cations, together with the identical systematic absences of space groups $I\bar{4}2m$ and $I\bar{4}$ did not allow discrimination between the possible zinc-blende-related superstructures. However, X-rays provide greater contrast between the Ag^+ and Zn^{2+} cations and refinement indicates that the kesterite structure is more likely, as a slightly lower goodness of fit parameter, χ^2, results.

Multibank neutron diffraction refinements were initiated using data from the highest resolution detector bank (2θ = 156°). The background was modelled using a reciprocal interpolation function and the peak shape described by a pseudo-Voigt function, with the coefficients included as variables in the refinement. Following refinement of lattice and atomic parameters, data from the remaining detector banks (2θ = 90°, 63° and 35°) were introduced sequentially. Both stannite ($I\bar{4}2m$) and kesterite ($I\bar{4}$) structural models were refined for all compositions. Initially, disorder associated with

View Article Online
DOI: 10.1039/C9CP03630J

each of the cation sites was considered through refinement of site occupancy factors, with the constraint that each site remained fully occupied.

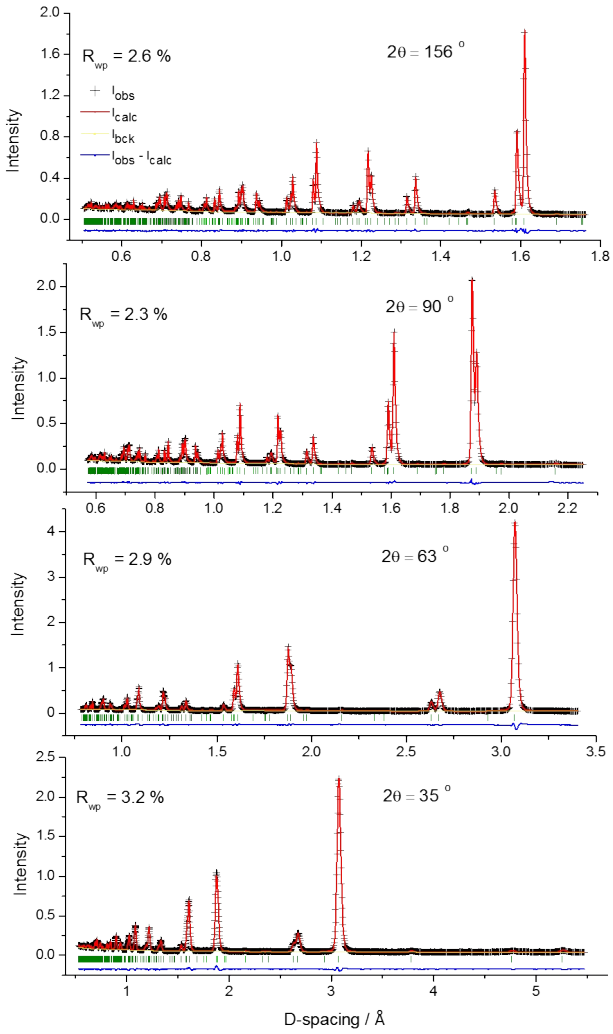

Figure 2. Multibank Rietveld refinement for Cu_2ZnGeS_4 using powder neutron diffraction data collected at room temperature ($\chi^2 = 2.8$). Observed (black crosses), refined (red solid lines) and difference (lower blue line) profiles. Reflection positions are marked by green vertical lines.

Rietveld analysis reveals that all quaternary compounds investigated here are better described in the space group $I\bar{4}$ than in $I\bar{4}2m$; consistent with the adoption of the kesterite structure for all compositions. A representative multibank Rietveld refinement

View Article Online
DOI: 10.1039/C9CP03630J

for Cu_2ZnGeS_4 is presented in Figure 2, while the remaining profiles are provided as ESI. Final lattice and atomic parameters resulting from Rietveld analysis of powder neutron diffraction data are presented in Tables 1 and 2.

Replacement of sulphur by the larger selenium anion increases both the *a* and *c* lattice parameters, leading to an increase in unit cell volume of *ca.* 16 % for a given combination of cations. The volume change induced by replacement of germanium with the larger tin cation for a given chalcogenide anion, is somewhat smaller at *ca*. 6 %. Significantly, whilst replacement of copper by the larger silver cation also increases the unit-cell volume by 12 – 14 %, this increase is primarily associated with an in-plane expansion: the *a* lattice parameter increasing by 6 - 7 %. In both Ag_2ZnSnS_4 and $Ag_2ZnSnSe_4$, the *c* lattice parameter is decreased slightly compared to their copper congeners, leading to a significant change in the *c*/2*a* ratio, which has a marked influence on the degree of order (*vide infra*).

Table 1: Lattice parameters determined from Rietveld analysis of powder neutron diffraction data for A_2ZnBQ_4(A = Cu, Ag; B = Ge, Sn; Q =S, Se)[a] compared with those obtained by DFT calculations (for configuration **K1**[b]).

	CZGS	CZGSe	CZTS	CZTSe	AZTS	AZTSe
			Neutron Diffraction			
a / Å	5.34333(2)	5.60873(2)	5.43218(3)	5.69544(5)	5.81261(3)	6.04419(3)
c / Å	10.51126(6)	11.04297(6)	10.8308(1)	11.3417(2)	10.77886(7)	11.30653(9)
c /2 *a*	0.984	0.985	0.997	0.996	0.927	0.936
V /Å^3	300.108(2)	347.388(3)	319.603(4)	367.902(6)	364.179(4)	413.052(5)
			DFT Calculations			
a /Å	5.365	5.657	5.461	5.744	5.850	6.109
c /Å	10.508	11.081	10.854	11.406	10.886	11.453
c /2*a*	0.979	0.979	0.994	0.993	0.930	0.937
V /Å^3	302.45	354.61	323.69	376.32	372.55	427.42

[a] CZTS, CZTSe, CZGS, CZGSe, AZTS and AZTSe denote Cu_2ZnSnS_4, $Cu_2SnSnSe_4$, Cu_2ZnGeS_4, $Cu_2ZnGeSe_4$, Ag_2ZnSnS_4 and $Ag_2ZnSnSe_4$ respectively.
[b] Configuration **K1** is defined below and shown in Figure 3.

View Article Online
DOI: 10.1039/C9CP03630J

Detailed analysis of site-occupancy-factor data reveals that the 2*b* site and 2*a* sites of the kesterite structure are fully occupied by the group 14 (Ge, Sn) and *A*- (Cu or Ag) cations respectively, in all compositions. However in the case of the copper-containing materials, there is anti-site disorder associated with the 2*c* and 2*d* positions (corresponding to cation planes at z = 0.25 and 0.75), the extent of which is dependent on the composition of the particular quaternary phase (Table 2).

Neutron diffraction reveals that in the kesterite Cu_2ZnGeS_4, the 2*c* site is occupied by *ca.* 67 % Cu and 33 % Zn: the occupancies being inverted at the 2*d* site. Structural refinement provides no evidence for anti-site defects involving the other cation sites in the kesterite structure (e.g. Cu/Zn on the 2*a* position, Cu/Ge or Zn/Ge on the 2*b* position), although the presence of low levels of occupancy of interstitial sites cannot be excluded completely. In addition, the 2*a* and 2*b* positions remain fully occupied by Cu and Ge cations respectively. While similar anti-site disorder is observed in the analogous selenide, its extent is reduced slightly, with the relative proportions of copper and zinc at the 2*c* site increased to *ca*. 71% and 29% respectively. Multibank refinements reveal a further marked reduction in the degree of Cu/Zn disorder, associated with cation planes at z = 0.25 and 0.75, for the two tin congeners, Cu_2ZnSnS_4 and $Cu_2ZnSnSe_4$. In Cu_2ZnSnS_4, only *ca.* 5.5% of the 2*c* sites are occupied by Zn cations, with the remainder of 94.5 % located at the 2*d* site; Cu cations occupying the remaining sites at each position. In the analogous selenide, these occupancies fall slightly to 92% and 8%. Again, there is no evidence for disorder associated with the remaining cation sites. The Cu/Zn disorder present in Cu_2ZnBQ_4 (B = Sn, Ge; Q = S, Se) contrasts with the behaviour of the Ag_2ZnSnQ_4 phases. Structural refinement using powder neutron and X-ray diffraction data simultaneously, demonstrates that the two silver-containing materials adopt a fully ordered kesterite structure. The extent of cation

View Article Online
DOI: 10.1039/C9CP03630J

disorder of Cu_2ZnSnS_4 has been shown to exhibit a dependence on thermal-history[26,44], particularly annealing temperature and rate of cooling. Although the synthetic procedure therefore has an impact on the cation ordering, the variations within the series of materials reported here can however be related to changes in sample composition, as all materials were prepared using slow cooling from elevated temperatures. In an effort to understand these composition-dependent changes in cation order, Density Functional Theory was used to explore the energies of the possible configurations.

Table 2: Key Refined Atomic Parameters Determined from Rietveld Refinement.[a]

Site	Parameter	CZGS	CZGSe	CZTS	CZTSe	AZTS	AZTSe
8*g*	x	0.246(3)	0.2479(5)	0.2423(5)	0.2382(5)	0.243(1)	0.2455(4)
	y	0.2650(9)	0.2584(1)	0.2375(4)	0.247(1)	0.2216(3)	0.2288(1)
	z	0.1224(2)	0.1243(1)	0.1269(5)	0.1287(1)	0.1289(3)	0.1288(1)
2*c*	SOF						
	(Cu/Ag)Zn	0.67(1)	0.71(1)	0.945(9)	0.92(2)	1.0(-)	1.0(-)
		0.33(1)	0.29(1)	0.055(9)	0.08(2)	0.0(-)	0.0(-)
2*d*	SOF						
	(Cu/Ag)Zn	0.33(1)	0.29(1)	0.055(9)	0.08(2)	0.0(-)	0.0(-)
		0.67(1)	0.71(1)	0.945(9)	0.92(2)	1.0(-)	1.0(-)

[a]*Space group:* $I\bar{4}$. (S, Se) on 8*g* (*x,y,z*); (Ge,Sn) on 2*b* (0,0,½); Cu on 2*a* (0,0,0); (*A*, Zn) on 2*c* (0,½,¼) and 2*d* (0,½,¾). All site occupancy factors are 1.0 unless otherwise stated.

Five symmetry-inequivalent configurations of the A^+ and Zn^{2+} cations may be identified (Figure 3) using the SOD program. Configurations **K1**, **K2** and **K3** are kesterite-like configurations, with no Zn^{2+} cations in the planes at $z = 0$ and $z = 0.5$. Configuration **S** corresponds to the stannite structure, in which all Zn^{2+} cations are located exclusively in the planes at $z = 0$ and $z = 0.5$. Configuration **M** mixes A^+ and Zn^{2+} cations in the planes at $z = 0$ and $z = 0.5$.

View Article Online
DOI: 10.1039/C9CP03630J

The calculated relative energies of these configurations, presented in Table 3, demonstrate that the **K1** configuration, which corresponds to the ordered kesterite structure, is the most stable for all compositions. This is in agreement with the results of powder neutron diffraction presented above. Calculated lattice parameters show excellent agreement with those determined experimentally (Table 1). In all cases the second most stable configuration is **K2**. This contains the same ordering pattern of A^{+} and Zn^{2+} cations within the planes located at z = 0.25 and z = 0.75 as that of the **K1** configuration but differs in the relative stacking of these two planes: in the **K2** configuration, Zn^{2+} cations in planes at z =0.25 and 0.75 are located directly above one another, whereas in **K1** the layers are displaced by (½, ½) with respect to each other, with the result that the Zn^{2+} cations are offset with respect to one another. The latter arrangement minimises the electrostatic $Zn^{2+}\cdots Zn^{2+}$ interactions and is therefore of lower energy. The stannite structure (configuration **S**) is always higher in energy than **K1** and **K2**, consistent with the results of experiment which provides no evidence for the adoption of this structure type. The other two configurations (**K3**, **M)** are of significantly higher energies for all compositions.

Figure 3. The five symmetry-inequivalent configurations for which DFT calculations were performed

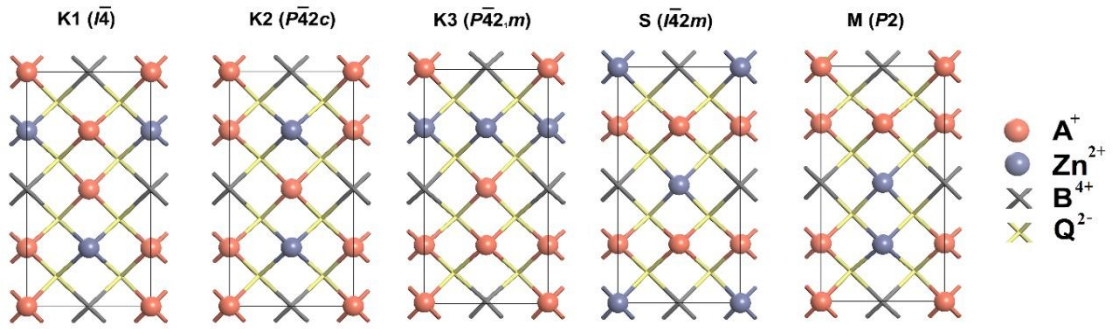

View Article Online
DOI: 10.1039/C9CP03630J

Table 3: Energies (meV) of the Five Configurations Presented in Figure 3. All Energies are Expressed Relative to that of the **K1** Configuration.

	K1	**K2**	**K3**	**S**	**M**
CZGS	0	8	401	86	310
CZGSe	0	5	231	78	171
CZTS	0	11	393	44	281
CZTSe	0	12	349	63	255
AZTS	0	211	496	324	590
AZTSe	0	186	445	355	1,726

Examination of the relative energies of **K1** and **K2** demonstrates that the energetic cost of vertically aligning the A^+ and Zn^{2+} cation distributions in the z = 0.25 and z = 0.75 planes is greater for A = Ag than for A = Cu. This can be related to the anisotropic expansion of the unit cell on moving from the copper-containing to the silver-containing phase discussed above. Although the larger Ag^+ cation has relatively little effect on the c lattice parameter, perpendicular to the cation planes, it produces an expansion of 6 – 7% of the a lattice parameter in the in-plane direction (Table 1). Expansion in a direction parallel to the cation planes, whilst maintaining an almost constant inter-planar separation, increases the electrostatic stabilization achievable by offsetting the $Zn^{2+}\cdots Zn^{2+}$ interactions in planes at z=0.25 and z=0.75 in the **K1** configuration. This leads to a greater stabilization of **K1** relative to **K2**. If cation disorder in the kesterite phases is considered in terms of a distribution of **K1** and **K2** configurations, the much higher energy of **K2** relative to **K1** in Ag_2ZnSnS_4 and $Ag_2ZnSnSe_4$ suggests that cation disorder of Ag and Zn cations within a plane will be energetically less favoured than the Cu/Zn disorder in the analogous copper chalcogenides, consistent with the fully ordered structure determined for Ag_2ZnSnS_4 and $Ag_2ZnSnSe_4$ by powder neutron diffraction. This conclusion is also consistent with the increase in Cu/Zn order that occurs when germanium is replaced with tin. The expansion of *ca*. 1.6 % in the in-plane, a, lattice

View Article Online
DOI: 10.1039/C9CP03630J

parameter suggests that the stabilization of **K1** relative to **K2** is increased in Cu_2ZnSnQ_4 compared to Cu_2ZnGeQ_4. This is borne out by the calculated energies of Table 3. However, it is notable that whilst the energy difference **K2 - K1** is increased in the tin-containing phases, the stabilization is markedly reduced compared to that resulting from the replacement of copper by silver. This may be associated with the fact that on going from Cu_2ZnGeQ_4 to Cu_2ZnSnQ_4, in addition to an in-plane expansion of *ca*. 1.6%, which stabilizes the ordered configuration (**K1**), there is an increase of *ca.* 3% in the inter-planar distances. This reduces the electrostatic stabilization achievable by displacing the next nearest-neighbour layers to minimise the $Zn^{2+}\cdots Zn^{2+}$ interactions and contrasts with the situation when copper is replaced by silver, where there is effectively no change in the *c* lattice parameter when the *a* lattice parameter increases.

Band gaps computed using the HSE functional (ESI) reveal that the replacement of S with Se tends to decrease the band gap, whereas the opposite effect is observed on substitution of Cu with Ag. These trends are broadly consistent with experimental data presented iin Table S1 of the ESI. Although the values of the band gap calculated for the **K1** and **K2** configurations are similar, only that for the **K1** configuration is relevant to the Ag-based materials, due to the high degree of ordering.

The results and analysis presented above suggest that inter-planar interactions are a significant factor behind the complete ordering observed in Ag-containing kesterites. However, intra-planar effects may also play a role. Their examination requires the use of an enlarged supercell. Therefore, we have performed calculations for the CZTS and AZTS compositions using a 2 × 2 × 1 supercell, in which *A*/Zn pairs were swapped both in the $z = 0.25$ and $z = 0.75$ planes (Figure 4). In the double-swapped configuration, the inter-planar interaction remains in the favourable offset configuration, and therefore the calculated swapping energy reflects only intra-planar effects.

View Article Online
DOI: 10.1039/C9CP03630J

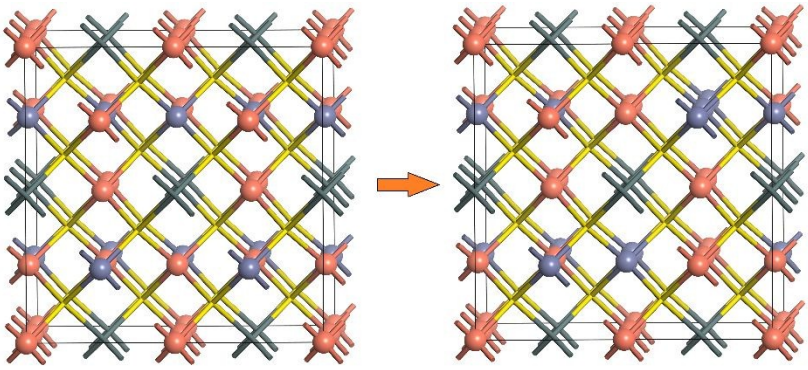

Figure 4. Double swapping of A/Zn cations in the **K1** Configuration

The energies of 400 meV per pair for Cu/Zn, and 540 meV per pair for Ag/Zn suggest that there is also an intra-planar effect that contributes to the higher degree of ordering observed in the Ag structures. The intra-planar effect is related to the much larger difference in ionic radius[45] between Ag^+ (1.0 Å) and Zn^{2+} (0.60 Å) compared to that between Cu^+ and Zn^{2+} (both ~0.60 Å). Therefore we conclude that both inter- and intra-planar effects contribute to the ordering of the Ag-containing structures. The energy differences associated with the inter-planar effects are however lower than the intra-planar energies, indicating the former may be the dominant affect, through the variation of the in-plane *a* lattice parameter. It has been suggested[46] that the suppression of *A*-Zn antisite defects when Cu is replaced with Ag may increase the open-circuit voltage V_{oc}. This result suggests that a potential route to engineer a higher degree of ordering in Cu kesterites, thereby addressing one of the factors that limit V_{oc} in a photovoltaic device, is through the application of tensile strain via an appropriate support during thin film growth, an idea that may merit further investigation.

Conclusions

In conclusion, this combined experimental and computational study demonstrates that all compositions in the series, A_2ZnBQ_4 (A = Cu, Ag; B = Sn, Ge; Q = S, Se), adopt the kesterite structure, which is shown to be lower in energy than alternatives, such as the

View Article Online
DOI: 10.1039/C9CP03630J

stannite structure, for all cation-anion combinations. The copper- and silver-containing materials exhibit contrasting behaviour, with the latter showing complete cation order. Cu/Zn anti-site disorder is observed in the copper-containing phases, the extent of which is affected by the identity of the group 14 cation. DFT reveals that the difference in behaviour between copper- and silver-containing phases is due to the accessibility of a second, relatively low energy, configuration in the former, in which next-nearest neighbour cation layers are vertically aligned with respect to one another. The disorder can thus be considered as a mixing of the ground state and next lowest energy configurations. On replacement of copper with silver there is an anisotropic expansion of the unit-cell, which increases the electrostatic stabilization achievable by offsetting the Zn^{2+}··Zn^{2+} interactions through adoption of a fully-ordered configuration. DFT reveals that this results in a marked increase in the energy separation between the ground state and low-energy configuration through which disorder occurs. Similar considerations account for the dependence of the extent of disorder on the identity of the group 14 cation.

Conflicts of interest

There are no conflicts to declare.

Acknowledgments

A.A. and P.M. acknowledge funding from the UK Engineering and Physical Sciences Research Council (EPSRC) Doctoral Training Partnership studentships. Calculations were performed using the U.K. National Supercomputing Facility ARCHER via our membership of the U.K. HPC Materials Chemistry Consortium (EPSRC Grant No. EP/L000202). The authors wish to thank the University of Reading for access to the

View Article Online
DOI: 10.1039/C9CP03630J

Chemical Analysis Facility for powder X-ray-diffraction measurements and the STFC for access to the ISIS Facility.

References

[1] S. Giraldo, Z. Jehl, M. Placidi, V. Izquierdo-Roca, A. Pérez-Rodríguez, E. Saucedo, *Adv. Mater*. 2019, **31**, 1806692.

[2] W. Wang, M.T. Winkler, O. Gunawan, T. Gokmen, T.K. Todorov, Y. Zhu and D.B. Mitzi, *Adv. Energy Mater.*, 2014, **4**, 1301465.

[3] M-L. Liu, I-W. Chen, F-Q. Huang and L-D. Chen, *Adv. Mater.*, 2009, **21**, 3808-3812.

[4] W.G. Zeier, A. LaLonde, Z.M. Gibbs, C.P. Heinrish, M. Panthöfer, G.J. Snyder and W. Tremel, *J. Amer. Chem. Soc.*, 2012, **134**, 7147-7154.

[5] X. Y. Shi, F. Q. Huang, M. L. Liu, and L. D. Chen, *Appl. Phys. Lett*., 2009, **94**, 122103.

[6] D. Zhang, H-C. Bai, Z-L. Li, J-L. Wang, G-S., Fu and S-F. Wang, *Chin. Phys. B*, 2018, **27**, 047206.

[7] M-L- Liu, F-Q Huang, L-D- Chen and I-W Chen, *Appl. Phys. Lett.,* 2009, **94**, 202103.

[8] I. Tsuji, Y. Shimodaira, H. Kato, H. Kobayashi and A. Kudo, *Chem. Mater*. 2010, **22**, 1402 – 1409.

[9] D.B. Mitzi, O. Gunawan, T.K. Todorov, K. Wang and S. Guha, *Sol. Energ. Mat. Sol C*, 2011, **95**, 1421–1436.

[10] T. Gokmen, O. Gunawan, T.K. Todorov and D.B. Mitzi, *Appl. Phys. Lett*, 2013, **103**, 103506.

[11] J.J.S. Scragg,, J. K. Larsen, M.. Kumar, C. Persson, J. Sendler, S. Siebentritt and C. Platzer Björkman, *Phys. Status Solidi B*, 2016, **253**, 247-254.

[12] S. Bourdais, C. Choné, B. Delatouche, A. Jacob, G. Larramona, C. Moisan, A. Lafond, F. Donatini, G. Rey, S. Siebentritt, A. Walsh and G. Dennler, *Adv. Energy Mater*., 2016, **6**, 1502276,

[13] J. Paier, R. Asahi, A. Nagoya and G. Kresse, *Phys. Rev. B*, 2009, **79***,* 115126.

[14] S. Siebebtritt and S. Schorr, *Prog. Photovolt. Res. Appl*., 2012, **20**, 512-519.

[15] A. Lafond, L. Choubrac, C. Guillot-Deudon, P. Deniard and S. Jobic, *Z. Anorg. Allg. Chem*., 2012**, 638**, 2571-2577**.**

[16] W. Y. Gong, T. Tabata, K. Takei, M. Morihama, T. Maeda and T. Wada, *Phys. Status Solidi C*, 2015, **12**, 700-703.

[17] J. M. Skelton, A. J. Jackson, M. Dimitrievska, S. K. Wallace and A. Walsh, *Apl Materials*, 2015, **3***,* 041102.

View Article Online
DOI: 10.1039/C9CP03630J

[18] D. F. Zou, G. Z. Nie, Y. Li, Y. Xu, J. G. Lin, H. R. Zheng and J. Y. Li, *RSC Adv.* 2015, **5**, 24908-24914.

[19] C. Raju, M. Falmbigl, P. Rogl, X. Yan, E. Bauer, J. Horky, M. Zehetbauer and R. C. Mallik, *AIP Adv.*, 2013, **3**, 032106.

[20] Y. K. Dong, H. Wang and G. S. Nolas, *Inorg. Chem.*, 2013, **52**, 14364-14367.

[21] R. Chetty, A. Ball, O.E. Femi, K. Chattopadhyay, R.C. Mallik, *J. Electron. Mater.* **2015**, *45*, 1625-1632.,

[22] W.G. Zeier, H. Zhu, Z.M. Gibbs, G. Cedre, W. Tremel and G.J. Snyder, *J. Mater. Chem. C*, 2014, **2**, 10189-10194.

[23] S. Chen, X. G. Gong, A. Walsh and S.-H. Wei, *Appl. Phys. Lett.*, 2009, **94**, 041903.

[24] S. Chen, A. Walsh, J.-H. Yang, X. G. Gong, L. Sun, P.-X. Yang, J.-H. Chu and S.-H. Wei, *Phys. Rev. B*, 2011, **83**, 165211.

[25] W. G. Zeier, C. P. Heinrich, T. Day, C. Panithipongwut, G. Kieslich, G. Brunklaus, G. J. Snyder and W. Tremel, *J. Mater. Chem. A*, 2014, **2**, 1790-1794.

[26] S. Schorr, *Sol. Energy Mater. Sol. Cells,* 2011, **95**, 1482-1488.

[27] M. Guc, S. Levcenko, V. Izquierdo-Roca, X. Fontane, E Arushanov and A. Perez-Rodriguez, *J. Appl. Phys.*, 2013, **114**, 193514.

[28] R. Gunder, J.A. Marquez-Prieto, G. Gurieva, T. Unold and S. Schorr, *CrystEngComm*, 2018, **20**, 1491-1498.

[29] A. Ritscher, A. Franz, S. Schorr and M. Lerch, *J. Alloys Compd.* 2016, **689**, 271-277.

[30] G. Gurieva, L.E.V. Rios, A. Franz, P. Whitfield and S. Schorr, *J. Appl. Phys.,* 2018, **123**, 161519.

[31] L. Choubrac, A. Lafond, C. Guillot-Deudon, Y. Moëlo and S. Jobic, *Inorg. Chem.*, 2012, **51**, 3346-3348.

[32] Z.-K. Yuan, S. Chen, H. Xiang, X.-G. Gong, A. Walsh, J.-S. Park, I. Repins, S.-H. Wei, *Adv. Funct. Mater.* 2015, **25**, 6733–6743

[33] DOI:10.5286/ISIS.E.67768949.

[34] A.C. Larson and R.B. Von Dreele, *Los Alamos National Laboratory Report* LAUR 1994, 86−784.

[35] G. Kresse and J. Furthmuller, *Phys. Rev. B*, 1996, **54**, 11169-11186.

[36] G. Kresse and J. Furthmüller, *Comp. Mater. Sci.*, 1996, **6**, 15-50.

[37] G. Kresse and J. Hafner, *Phys. Rev. B*, 1994, **49**, 14251-14269.

[38] J. Heyd, G. E. Scuseria and M. Ernzerhof, *J Chem. Phys.*, 2003, **118**, 8207-8215.

[39] J. Heyd, G. E. Scuseria and M. Ernzerhof, *J Chem. Phys.*, 2006, **124**, 219906.

View Article Online
DOI: 10.1039/C9CP03630J

[40] T. M. Henderson, J. Paier and G. E. Scuseria, *Phy. Status Solidi B,* 2011, **248**, 767-774.

[41] G. Kresse and D. Joubert, *Phys .Rev. B*, 1999, **59**, 1758-1775.

[42] P. E. Blochl, *Phys. Rev. B*, 1994, **50**, 17953-17979.

[43] R. Grau-Crespo, S. Hamad, C. R. A. Catlow and N. H. de Leeuw, *J. Phys-Condens. Mat.*, 2007, **19**, 256201.

[44] A. Ritscher, M. Hoelzel and M. Lerch, *J. Solid State Chem.*, 2016, **238**, 68–73.

[45] R.D. Shannon, *Acta Crystallogr. Sect. A,* 1976, **32**, 751-767.

[46] C. Maa, H. Guoa, K. Zhanga, N. Yuana and J. Dinga, *Mater. Lett.*, 2017, **186**, 390–393.

View Article Online
DOI: 10.1039/C9CP03630J

Table of Contents Entry

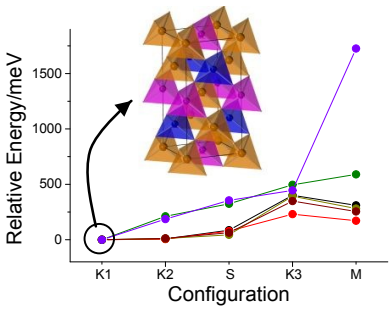

Neutron diffraction coupled with Density Functional Theory provides new insights into the structural features of quaternary chaclogenides